Research Article | Vol. 28, No. 6 / 16 March 2020 / Optics Express 7906
Optics EXPRESS

Controllable coupling between an ultra-high-Q microtoroid cavity and a graphene monolayer for optical filtering and switching applications

HUIBO FAN,[1,2] XUN ZHANG,[1] JINYI ZHAO,[1] SHENGJUN LI,[1] SHIYUE HUA,[1] MINGMING ZHAO,[1] YONG HU,[1] WENJIE WAN,[3] YANHUA ZHAI,[4] JIANMING WEN,[4] XIAOSHUN JIANG,[1,*] AND MIN XIAO[1,5]

[1]*National Laboratory of Solid Sate Microstructures, College of Engineering and Applied Sciences, School of Physics, Nanjing University, Nanjing 210093, China*
[2]*College of Physics Science and Technology, Yangzhou University, Yangzhou 225002, China*
[3]*The State Key Laboratory of Advanced Optical Communication Systems and Networks, University of Michigan-Shanghai Jiao Tong University Joint Institute, Shanghai Jiao Tong University, Shanghai 200240, China*
[4]*Department of Physics, Kennesaw State University, Marietta, Georgia 30060, USA*
[5]*Department of Physics, University of Arkansas, Fayetteville, Arkansas 72701, USA*
[*]*jxs@nju.edu.cn*

Abstract: Whispering-gallery-mode optical microresonators have found impactful applications in various areas due to their remarkable properties such as ultra-high quality factor (Q-factor), small mode volume, and strong evanescent field. Among these applications, controllable tuning of the optical Q-factor is vital for on-chip optical modulation and various opto-electronic devices. Here, we report an experimental demonstration with a hybrid structure formed by an ultra-high-Q microtoroid cavity and a graphene monolayer. Thanks to the strong interaction of the evanescent wave with the graphene, the structure allows the Q-factor to be controllably varied in the range of $3.9 \times 10^5 \sim 6.2 \times 10^7$ by engineering optical absorption via changing the gap distance in between. At the same time, a resonant wavelength shift of 32 pm was also observed. Besides, the scheme enables us to approach the critical coupling with a coupling depth of 99.6%. As potential applications in integrated opto-electronic devices, we further use the system to realize a tunable optical filter with tunable bandwidth from 116.5 MHz to 2.2 GHz as well as an optical switch with a maximal extinction ratio of 31 dB and response time of 21 ms.

1. Introduction

By confining light in a tiny volume with high Q-factor so as to enhance the interaction of light with matters within or surrounding the cavity, whispering-gallery-mode (WGM) microcavities have shown promising applications as a crucial element for a variety of devices ranging from micro-lasers, biosensors, add-drop filters, micro-modulators, to Kerr optical frequency combs [1–8]. Owing to the full compatibility with the mature CMOS procedure, they are becoming the basic building blocks of integrated photonic systems [1]. As such, over a decade tremendous progress has been made in the development of miniature photonic information processing technologies based upon microscale high-Q microcavities [9]. Nevertheless, many of these applications rely on the capability of tuning the Q-factors as well as shifting the resonant wavelengths. For instance, high-Q microcavities are highly sensitive to various environmental factors such as temperature, humidity, and any particles or absorbers [10–12]. To enforce the sensing applications, new methods including photothermal mapping and phase shift microcavity ring down spectroscopy have recently been exploited to change Q-factor and resonant wavelength [13–15]. Alternatively, the ability of controllably tuning these two factors becomes critical for a

#388472 https://doi.org/10.1364/OE.388472
Journal © 2020 Received 16 Jan 2020; revised 22 Feb 2020; accepted 24 Feb 2020; published 2 Mar 2020

Optics EXPRESS

wide range of applications, e.g., in the design of ultra-short pulsed lasers and optical modulators. Although some progress has been made in utilizing a broadband absorber to reach the goals [16]. Yet, it is still quite challenging to realize these opto-electronic devices with desired tunability, partly due to the technical difficulty in integrating high-Q microcavities with such absorption media in a controllable way.

On the other hand, given excellent optical properties including linear optical absorption [17–19], graphene monolayers as ideal two-dimensional quantum materials have aroused great interest in many photonic device applications, such as polarizers [20], photodetectors [21], modulators [22–25], pulsed lasers [26] and optical switches [27,28]. However, due to technical complexity, these devices are usually unreachable or unoptimizable in conventional material systems [29,30]. Moreover, for various photonic applications [30–34], there is a high demand for transferring and integrating graphene efficiently onto fiber end faces or chip-based photonic devices, such as waveguides and optical microcavities. Along this direction, recent efforts are made towards optoelectronic devices based upon a graphene-clad photonic crystal nanocavity to achieve resonant optical bistability, regenerative oscillation, and four-wave mixing [30]. Besides, a graphene electro-optic modulator rooted in a silicon nitride microring resonator was also demonstrated where the modulation bandwidth of 30 GHz was reported [16]. Despite these impressive results, it is still lack of a systematic study of the light-matter interaction between an ultra-high-Q microcavity and graphene, especially the realization of a tunable interaction strength.

By using graphene as a tunable absorber, here we report an experimental demonstration of such a controllable coupling based on a hybrid structure composed of an ultra-high-Q microtoroid cavity and a graphene monolayer through changing the Q-factor in orders of magnitude. The schematic of the experimental setup is shown in Fig. 1(a). The scheme is capable of accurately controlling the distance between the microtoroid and graphene via the high-precision piezoelectric stages. Thanks to the optical absorption of graphene induced by the strong evanescent wave outside of the microtoroid cavity, the Q-factor can be altered from 6.2×10^7 to 3.9×10^5 as gradually reducing the microtoroid-graphene gap spacing. Meanwhile, the microcavity resonant wavelength is shifted towards the longer wavelength, which yields a maximal shift of about 32 pm, which is in agreement with the simulated result of 41 pm. As the graphene monolayer is gradually moved away from the microtoroid surface, the microcavity Q-factor as well as its resonant wavelength are restored to their original values eventually. In addition, we demonstrate the critical coupling using this hybrid structure with the coupling depth of 99.6%. Besides, we further experimentally realize a tunable filter with a variable bandwidth in the range of 116.5 MHz ~ 2.2 GHz, and an optical switch with a maximal extinction ratio of 31 dB and response time of 21 ms. All these demonstrations indicate that our hybrid structure provides a practical reference for realization of integrated opto-electronic devices including on-chip optical modulators and filters.

2. Simulation and principle

Since the field distribution of the cavity mode is essential for the potential applications of the demonstrated hybrid structure, we first carried out a theoretical analysis on the optical properties of this hybrid system, and in particular, we focused on the additional losses of different cavity resonant modes induced by the optical absorption of the graphene monolayer. In the theory, a finite-element simulation was conducted in which the graphene monolayer was treated as a 0.35-nm-thick dielectric layer, and the corresponding optical properties were taken from [35]. For the microtoroid cavity used in the experiment, its principal (denoted by D in Fig. 2(a)) and minor (d) diameters are, respectively, measured to be 56 μm and 6 μm, which have been used in the simulation. The intrinsic loss of the hybrid system comes mainly from two sources, that is, the intrinsic loss of the microcavity and the extra loss caused by the graphene. Mathematically,

Optics EXPRESS

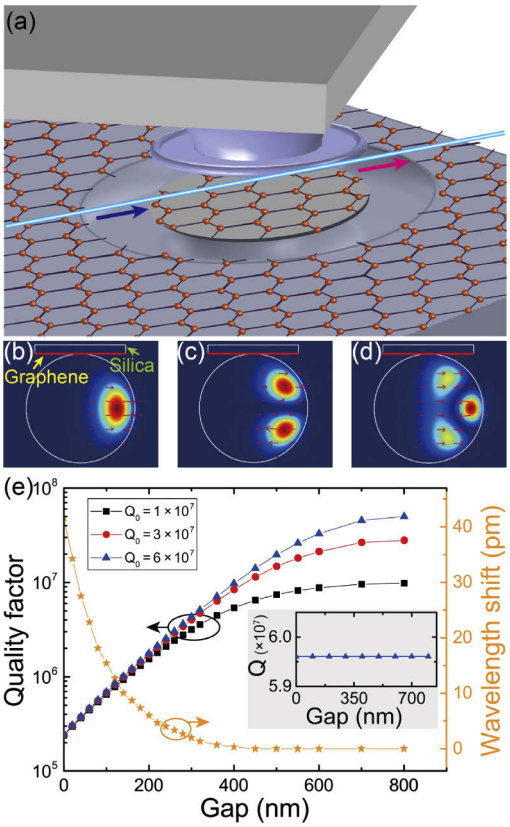

Fig. 1. (a) The schematic of the proposed hybrid structure containing microtoroid and graphene. (b-d) Optical profiles of fundamental, second-order, and third-order TE modes of the fabricated microtoroid, respectively. (e) Numerical simulations of Q-factor and resonant wavelength shift as a function of the gap distance for the case of Fig. 1(c). As one can see, when the graphene was gradually moved close to the microtoroid, Q decreases to the minimum of 2.3×10^5 under different Q_0 values of 1×10^7, 3×10^7, and 6×10^7, respectively. The maximal resonant wavelength shift is 41 pm. The inset shows the comparison of Q-factor variation of second-order TE mode in this hybrid structure without coating graphene for $Q_0 = 6 \times 10^7$.

this intrinsic loss is modeled via the Q-factors by the relationship $1/Q = 1/Q_0 + 1/Q_{gra}$, where Q_0 is the intrinsic Q factor of the microcavity while Q_{gra} is the effective Q factor describing the graphene absorption. In the simulation, it was noticed that in comparing with high-order modes, the cavity fundamental mode was located near the middle of the ring, and yielded a weaker coupling with the graphene. For instance, the Q-factors of fundamental modes are decreased to be the minimum of 3.0×10^6 and 2.0×10^7 for the transverse electric (TE) and transverse magnetic (TM) modes, respectively, when the gap distance between microtoroid and graphene gradually approaches to zero. The fundamental TE mode profile is schematically illustrated in Fig. 1(b).

In contrast, the third-order modes were distributed near the edge of the ring and consequently, yielded stronger coupling with the graphene with a larger variation of the Q-factor. In this work, the Q-factors were reduced to the minimum of 8.8×10^4 and 6.0×10^5, respectively, for the TE and TM modes as the microtoroid-graphene gap decreases to zero. Figure 1(d) depicts such third-order TE mode distribution. As a comparison, Fig. 1(c) shows the second-order TE mode

Optics EXPRESS

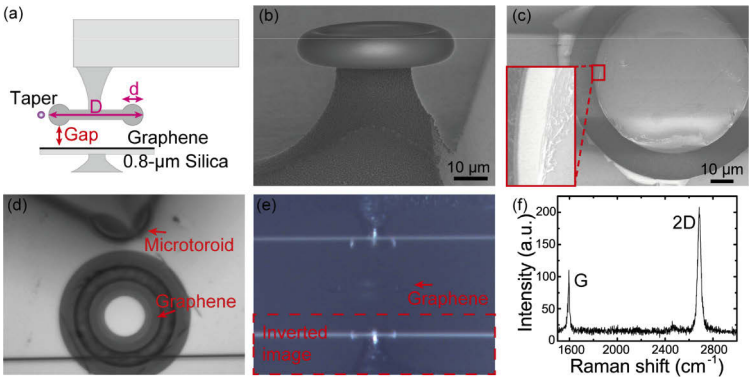

Fig. 2. (a) Side-view of the experimental setup. Here, the microtoroid was inverted for the convenience of observation and measurement. (b) Scanning electron micrograph (SEM) of the microtoroid fabricated on the corner of a silicon chip. (c) Top-view SEM of a specially-designed silica microdisk coated with graphene monolayer. Inset: magnified image of the microdisk edge. (d-e) Top-view and side-view optical microscope images of the hybrid structure, respectively. (f) Raman spectrum of graphene monolayer coated on the microdisk for the laser wavelength at 532 nm.

profile subject to the interaction with the graphene, where Q-factor drops to approximately 2.3×10^5 (1.7×10^6 for the TM mode); the corresponding simulated data was presented in Fig. 1(e). Moreover, we also performed the simulation (inset of Fig. 1(e)) of the coupling between the second-order TE mode of the microtoroid and the pure silica substrate film (without graphene) with a thickness of 0.8 μm, which indicates that the silica substrate has no influence on the Q-factor and the resonance wavelength of the hybrid structure. Physically, it is expected that the total Q is dominated by Q_0 when graphene is far away from the microtoroid, but dominated by Q_{gra} when the gap is small owing to the strong graphene absorption. In addition, the gap reduction also leads to the resonant wavelength shift towards long wavelength. As shown in Fig. 1(e), we have observed the maximal wavelength shift of ~ 41 pm for the second-order TE mode in the proposed compound system, owing to the increase of the effective refractive index.

3. Experimental results and discussion

To verify our numerical predictions, an ultra-high-Q microtoroid resonator was fabricated through a series of steps which involve photolithography, hydrofluoric acid etching, xenon difluoride etching, and carbon dioxide laser reflow [9]. In our design, the ultra-high-Q microcavity was fabricated on the corner of a silicon chip to ease the measurements [36,37], whose scanning electron microscopy (SEM) image was given in Fig. 2(b). The graphene monolayer was provided by XFNANO Materials Tech Co., Ltd. (Nanjing, China) and grown via chemical vapor deposition (CVD). In the experiment, this graphene monolayer was mechanically transferred to a special-designed silica substrate, i.e., a silica microdisk with a diameter of ~ 60 μm and a thickness of 0.8 μm [32], see Figs. 2(c) and 2(d). Specifically, Fig. 2(c) shows the top-view SEM image of the graphene coated on the microdisk. The corresponding Raman spectrum measured at the wavelength of 532 nm for the graphene is shown in Fig. 2(f). Here, the 'G' and '2D' peaks both follow the Lorentzian lineshapes and are, respectively, located at 1593.5 cm^{-1} and 2684.6 cm^{-1}. Based on the relative intensities of the G and 2D peaks as well as their Lorentzian profiles, the presence of only a single-layer graphene is thus confirmed [38]. To provide a necessary protection during the transfer process, a poly methyl methacrylate (PMMA) layer was first coated on the graphene and then was dissolved by acetone after the transfer process. The specially-designed

Optics EXPRESS

silica microdisk substrate with 0.8-μm thickness was used to exclude the adverse effects, such as the absorptions of silica and silicon substrates. These procedures ensure that only controllable coupling between the microtoroid and graphene is obtained in the experiment. To form the proposed hybrid scheme, as illustrated in Fig. 2(a), the microtoroid cavity was inversely mounted for the convenience of observation and measurement. The gap spacing between the microtoroid and the graphene monolayer was precisely controlled through two piezoelectric stages (Attocube ANP101 with a resolution of ~ 1 nm). The coupling between the graphene monolayer and the microcavity was then investigated by measuring the optical transmission spectra of the launched light through a fiber taper [39] with different coupling distances at the telecom band 1550 nm. Here, the diameter of the fiber taper employed in the experiment is around 1-2 μm. However, thick fiber-taper designs with long period fiber gratings can also be used to achieve a more robust coupling [40,41]. To adjust the input light beam, a polarization controller and a variable optical attenuator were employed in the optical path. By moving graphene towards the microtoroid surface, the gap reduction leads to the growth of the cavity loss, then the variations of quality factor and resonant wavelength. Figures 2(d) and 2(e) are the top-view and side-view optical microscope images of the hybrid structure, respectively.

In order to characterize this microtoroid-graphene composite structure, the graphene monolayer was initially placed far away from the microtoroid to ensure no influence of graphene absorption on the cavity modes. Under such an arrangement, the input laser was gradually scanned to identify an appropriate cavity mode with a high optical Q-factor, which gave an initial intrinsic Q-factor of 6.2×10^7 at the 1570.0 nm wavelength. Subsequently, the graphene was slowly moved close to the microtoroid surface, and the set of corresponding transmission spectra coupled outward from the cavity was recorded via a digital oscilloscope. The reduced gap resulted in the increased interaction between the evanescent wave and electron transition in graphene, which in turn broadened the cavity resonance linewidth. Consequently, this led to a significant reduction in the Q-factor. As expected, the optical loss of the hybrid system reached the maximum when graphene exactly touched the microtoroid (i.e., the gap vanished), and yielded the smallest Q-factor of 3.9×10^5, which indicate the Q-factor of the hybrid system in mainly depend on the absorption of the graphene. By reversing the procedure through moving the graphene away from the cavity, interestingly, Q-factor could reinstate its original value of 6.2×10^7 in the end.

The evolution of the transmission spectra was displayed in Fig. 3(a) in terms of the gap separation distance, which clearly showed the linewidth broadening along with the wavelength shift of cavity resonance. The slightly asymmetric transmission at small gap spacing between graphene and microtoroid, may attribute to the interference between the reflected signal in the optical path to the cavity mode. The corresponding variations of the measured intrinsic Q-factors and the resonant wavelength shift were plotted in Figs. 3(b) and 3(c), respectively. Note that during the intrinsic Q-factor measurement of the compound system, the distance between the fiber taper and the microtoroid was also accordingly changed (within 1 μm) to obtain the proper coupling for different microtoroid-graphene gap spacing. It is worthwhile to emphasize again that throughout the whole observation, the optical Q-factor of the system can be reversibly altered in the range of 6.2×10^7 to 3.9×10^5 without degradation. In addition, to ensure that the observed Q variation was unaffected by the silica substrate film under the graphene, a similar silica microdisk with no graphene coating was fabricated and used for the experimental calibration procedure described above. It turns out that no obvious spectral changes were recorded in the transmission spectrum, implying no additional loss induced by the silica film. From Fig. 3(a), it becomes also apparent that owing to the optical absorption of graphene, the microtoroid resonant wavelength was shifted to the longer wavelength band by gradually diminishing the microtoroid-graphene gap, and vice versa. This property is highly beneficial for the designs of on-chip optical modulation as well as optical switching. The obtained maximal resonant wavelength shift was approximately 32 pm. For comparison, the resonant wavelength shift in the latter experiment with the graphene-free

Optics EXPRESS

microdisk was less than 1 pm, which in turn highlights that the resonant wavelength change in the former experiment was indeed a result of the coupling between the cavity mode and the graphene monolayer. Moreover, we also measured the Q-factor of the microtoroid cavity coated by a graphene monolayer, which was around 10^3, few orders of magnitude smaller than its initial Q value. This alternatively implies the superiority of the reported hybrid structure with controllable coupling between high-Q microcavity and graphene.

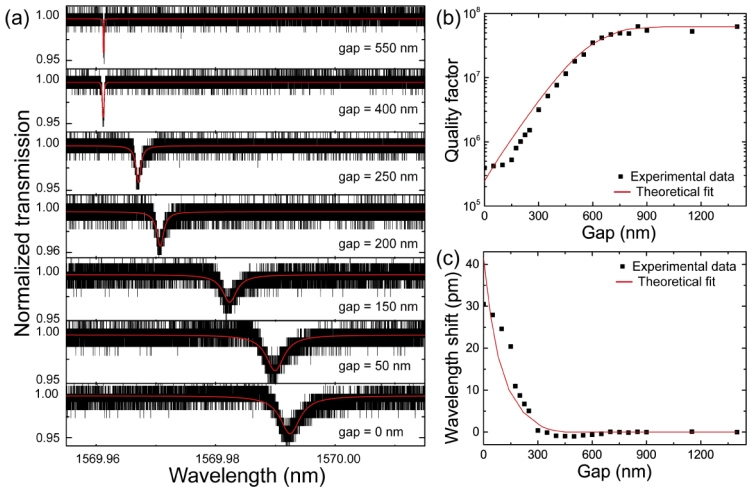

Fig. 3. (a) Evolution of transmission spectra in terms of the gap spacing between graphene and microtoroid. (b-c) The extracted Q-factor and the resonant wavelength shift of the microtoroid versus the microtoroid-graphene gap distance. Red curves are the theoretical fits obtained from the finite-element simulations.

By comparing the experiment data with the theoretical simulations in Figs. 3(b) and 3(c), we found that the employed cavity mode turns out to be the second-order TE mode (illustrated in Fig. 1(c)). This was further confirmed by moving the fiber taper in the vertical direction around the microtoroid while monitoring the transmission changes, which exhibited two critical coupling conditions [42]. A slight difference appeared between the simulation and experiment when the microtoroid-graphene gap becomes vanishing. Such a discrepancy may stem from the incomplete or uneven coating of graphene on the microdisk surface during the fabrication process, as evidenced in Fig. 2(c), or the contamination of the graphene during the measurement due to the repeated contact to the microtoroid cavity, or the non-uniform structure of the microtoroid induced by the CO_2 laser reflow for the fabrication of the microcavity. As a result, there was a slight degradation of the graphene absorption in the designed hybrid structure. Similar results were also observed in the transmission spectra associated with other cavity modes.

It is well-known that the critical coupling, as a unique property for the waveguide-coupled-microcavity system, occurs when the external coupling rate between waveguide and microcavity equals to the intrinsic decay rate of microcavity [39,43]. In other words, critical coupling ideally produces zero transmission output on resonance. This behavior can be used for optical filtering or effective optical power buildup in the microcavity [44,45]. In previous works, the critical coupling was demonstrated in the GaAs disk-nanowaveguide coupling system [46] or in the graphene coupling photonic crystal slab system [47] by controlling the coupling distance or the decay rate of the cavity mode, respectively. Interestingly, the microtoroid-graphene hybrid structure developed here is another ideal setup to look at the critical coupling condition so as to the potential application of tunable filter. To approach this coupling condition experimentally, prior to the reduction of the microtoroid-graphene gap, the taper-microtoroid subsystem was

Optics EXPRESS

first biased into the over-coupled regime. Then, the optical transmission spectra were monitored by decreasing the microtoroid-graphene gap while fixing the distance between fiber taper and microtoroid. Figure 4(a) shows the relationship of the evolved resonant transmissions and the varied microtoroid-graphene gap. As one can see, the critical coupling point was reached at a coupling depth of 99.6% when the gap spacing was ~ 1 μm. Since the cavity linewidth would be affected by the light-graphene interaction, it is instructive to understand the power transmission on resonance as a function of the resonant mode linewidth. After critical coupling, the linewidth would be broadened along with moving graphene close to the microtoroid [39]. This trend has been verified in our experiment and the comparison between theory and experiment is provided in Fig. 4(b). We notice that for the linewidth larger than 0.6 GHz (corresponding to $Q = 3.2 \times 10^5$), as the microtoroid-graphene gap spacing became close to zero, there was a slight deviation between the experiment and simulation due to the large fluctuation in the transmission spectra. Being a potential application exploiting the critical coupling effect, we utilized this hybrid structure to implement a bandwidth-tunable filter. The experimental results are shown in Fig. 5. As one can see, by decreasing the gap, the full width at half maximum (FWHM) of the transmitted spectrum becomes enlarged. In this work, we have achieved the bandwidth tunable optical filter with a bandwidth from 116.5 MHz up to 2.2 GHz.

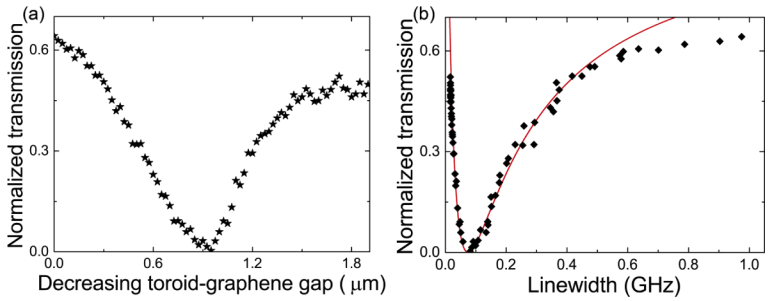

Fig. 4. (a) Normalized transmission versus the gap separation between graphene and microcavity. The minimum transmission corresponds to the critical coupling point. (b) Normalized transmission versus the linewidth (FWHM) of resonant mode. The red curve was calculated from the model given in [39].

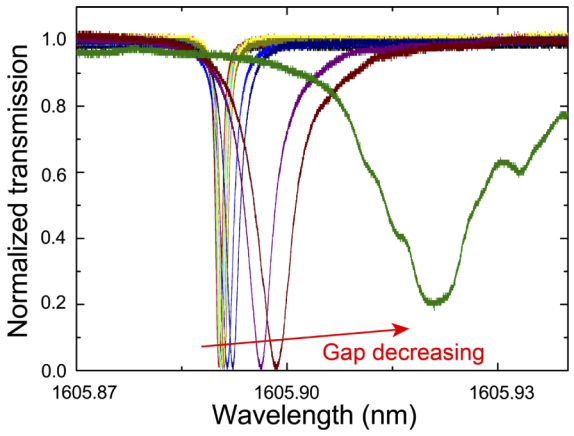

Fig. 5. By tuning the gap spacing, the large variations of the linewidth and resonant wavelength shift in transmission spectrum are used to realize a tunable optical filter with a tunable bandwidth from 116.5 MHz to 2.2 GHz.

Optics EXPRESS

Given the easy access to the resonant wavelength shift and critical coupling, the scheme can be considered for another potential application in optical switching. In contrast to the previous graphene-based optical switching based on the electro-refractive effect of graphene [28,34,48,49], in spite of the limited bandwidth, our scheme provides an easy approach with low insertion loss and high extinction ratio. The experimental results are given in Fig. 6. Experimentally, the graphene monolayer was first placed far away from the microtoroid cavity. A signal light operated at the wavelength of 1575.2 nm was tuned to the resonance of the cavity mode to yield near zero transmittance. By quickly moving the graphene close enough to the microtoroid surface, a near unity transmission at the input signal wavelength was then observed because of the off resonance (between the microtoroid and fiber taper) induced by the resonant wavelength shift. Next, a proper rectangular wave with tunable pulse width at a fixed 1-Hz repetition rate was utilized to accurately control the high-precision piezoelectric stage for the fine scanning of the microtoroid-graphene gap within the range of 722 nm ~ 0 nm, as indicated by the red curve in Fig. 6(b). The repeated back-forth shifting of the resonant wavelength thus functions as optical switching. The experimental data is present in Fig. 6(a) where the maxima of the normalized transmission spectra drop sharply from unit to almost 0 when the pulse width of the rectangular wave changes from 0.5 s to 0.01 s. Such a dramatic change gives rise to a high extinction ratio with the maximum of 31 dB, as shown in Fig. 6(c). Note that Fig. 6(b) also shows the enlarged output spectrum with the pulse width of 0.5 s, implying the response time of 21 ms. Here, this response time is mainly limited by the response speed of the employed high-precision piezoelectric displacement, which can be further increased by faster tuning the position of the graphene such as using opto-mechanical effect [2].

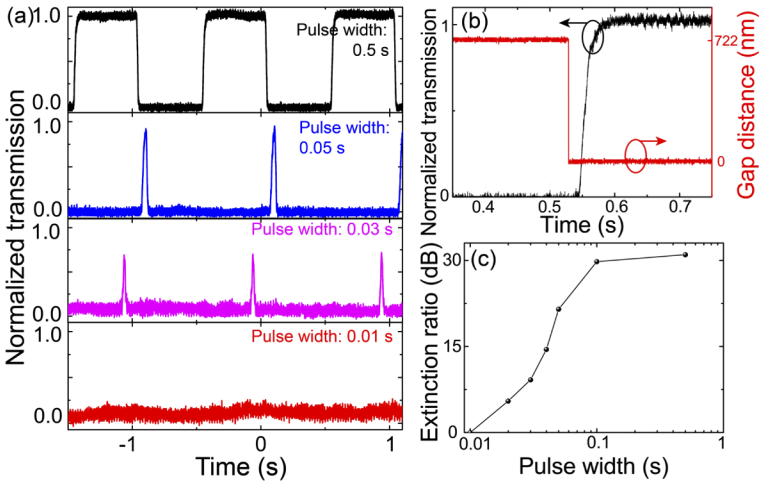

Fig. 6. (a) Normalized transmission spectra of the demonstrated optical switch by scanning the microtoroid-graphene gap in the range of 722 nm ~ 0 nm with different pulse widths of a rectangular wave at the fixed 1-Hz repetition rate. (b) Amplified transmission spectrum for the 0.5 s pulse width of a rectangular wave. (c) The extinction-ratio change in Fig. 6(a) as a function of the pulse width, with the maximum of 31 dB.

4. Conclusion

In summary, by designing a hybrid structure consisting of an ultra-high-Q silica microtoroid cavity and a monolayer of graphene, we have carried out a systematic investigation on the variations of Q-factor and cavity resonant wavelength shift induced by the controllable optical absorption of the graphene. In the experiment, the optical Q-factor could be reversibly changed

Optics EXPRESS

between 6.2×10^7 and 3.9×10^5 through tuning the gap separation between the two subsystems. Due to the cavity evanescent wave interacting with the graphene, the cavity resonant wavelength is also shifted up to 32 pm. Besides, the critical coupling condition can be well approached in this system with a sufficiently high coupling depth of 99.6%. As potential applications, we have further demonstrated a tunable optical filter with a variable bandwidth in the range of 116.5 MHz ~ 2.2 GHz as well as an optical switch with a maximal extinction ratio of 31 dB and response time of 21 ms. These demonstrations clearly show that the microcavity-graphene hybrid design could become an excellent platform for the realization of integrated opto-electronic devices such as on-chip optical filters and optical switching. Additionally, we anticipate that this hybrid structure would find applications in cavity-enhanced nonlinear optics of the 2D layered materials [50] and low-threshold micro-lasers by replacing the graphene monolayer with other transition metal dichalcogenides (TMDC) gain materials [51,52].

Funding

National Key Research and Development Program of China (2016YFA0302500,2017YFA0303703); National Natural Science Foundation of China (11804292, 61922040); Fundamental Research Funds for the Central Universities (021314380149); National Science Foundation (1806519, EFMA-1741693); Kennesaw State University.

Disclosures

The authors declare no conflicts of interest.

References

1. K. J. Vahala, "Optical microcavities," Nature **424**(6950), 839–846 (2003).
2. M. Aspelmeyer, T. J. Kippenberg, and F. Marquardt, "Cavity optomechanics," Rev. Mod. Phys. **86**(4), 1391–1452 (2014).
3. M. L. Gorodetsky, A. A. Savchenkov, and V. S. Ilchenko, "Ultimate Q of optical microsphere resonators," Opt. Lett. **21**(7), 453–455 (1996).
4. F. Shu, X. Jiang, G. Zhao, and L. Yang, "A scatterer-assisted whispering-gallery-mode microprobe," Nanophotonics **7**(8), 1455–1460 (2018).
5. F. Monifi, J. Friedlein, ŞK Ozdemir, and L. Yang, "A Robust and Tunable Add–Drop Filter Using Whispering Gallery Mode Microtoroid Resonator," J. Lightwave Technol. **30**(21), 3306–3315 (2012).
6. T. J. Kippenberg, A. L. Gaeta, M. Lipson, and M. L. Gorodetsky, "Dissipative Kerr solitons in optical microresonators," Science **361**(6402), eaan8083 (2018).
7. A. L. Gaeta, M. Lipson, and T. J. Kippenberg, "Photonic-chip-based frequency combs," Nat. Photonics **13**(3), 158–169 (2019).
8. J. Ma, L. Xiao, J. Gu, H. Li, X. Cheng, G. He, X. Jiang, and M. Xiao, "Visible Kerr comb generation in a high-Q silica microdisk resonator with a large wedge angle," Photonics Res. **7**(5), 573–578 (2019).
9. D. K. Armani, T. J. Kippenberg, S. M. Spillane, and K. J. Vahala, "Ultra-high-Q toroid microcavity on a chip," Nature **421**(6926), 925–928 (2003).
10. Q. Ma, T. Rossmann, and Z. Guo, "Whispering-gallery mode silica microsensors for cryogenic to room temperature measurement," Meas. Sci. Technol. **21**(2), 025310 (2010).
11. S. Yang, Y. Wang, and H. Sun, "Advances and Prospects for Whispering Gallery Mode Microcavities," Adv. Opt. Mater. **3**(9), 1136–1162 (2015).
12. A. M. Armani, R. P. Kulkarni, S. E. Fraser, R. C. Flagan, and K. J. Vahala, "Label-Free, Single-Molecule Detection with Optical Microcavities," Science **317**(5839), 783–787 (2007).
13. K. D. Heylman and R. H. Goldsmith, "Photothermal mapping and free-space laser tuning of toroidal optical microcavities," Appl. Phys. Lett. **103**(21), 211116 (2013).
14. M. I. Cheema, S. Mehrabani, A. A. Hayat, Y.-A. Peter, A. M. Armani, and A. G. Kirk, "Simultaneous measurement of quality factor and wavelength shift by phase shift microcavity ring down spectroscopy," Opt. Express **20**(8), 9090–9098 (2012).
15. L. Shao, X.-F. Jiang, X.-C. Yu, B.-B. Li, W. R. Clements, F. Vollmer, W. Wang, Y.-F. Xiao, and Q. Gong, "Detection of Single Nanoparticles and Lentiviruses Using Microcavity Resonance Broadening," Adv. Mater. **25**(39), 5616–5620 (2013).
16. C. T. Phare, Y.-H. Daniel Lee, J. Cardenas, and M. Lipson, "Graphene electro-optic modulator with 30 GHz bandwidth," Nat. Photonics **9**(8), 511–514 (2015).

Optics EXPRESS

17. R. R. Nair, P. Blake, A. N. Grigorenko, K. S. Novoselov, T. J. Booth, T. Stauber, N. M. R. Peres, and A. K. Geim, "Fine Structure Constant Defines Visual Transparency of Graphene," Science **320**(5881), 1308 (2008).
18. J. M. Dawlaty, S. Shivaraman, J. Strait, P. George, M. Chandrashekhar, F. Rana, M. G. Spencer, D. Veksler, and Y. Chen, "Measurement of the optical absorption spectra of epitaxial graphene from terahertz to visible," Appl. Phys. Lett. **93**(13), 131905 (2008).
19. F. Bonaccorso, Z. Sun, T. Hasan, and A. C. Ferrari, "Graphene photonics and optoelectronics," Nat. Photonics **4**(9), 611–622 (2010).
20. Q. Bao, H. Zhang, B. Wang, Z. Ni, C. H. Y. X. Lim, Y. Wang, D. Y. Tang, and K. P. Loh, "Broadband graphene polarizer," Nat. Photonics **5**(7), 411–415 (2011).
21. F. Xia, T. Mueller, Y.-M. Lin, A. Valdes-Garcia, and P. Avouris, "Ultrafast graphene photodetector," Nat. Nanotechnol. **4**(12), 839–843 (2009).
22. M. Liu, X. Yin, E. Ulin-Avila, B. Geng, T. Zentgraf, L. Ju, F. Wang, and X. Zhang, "A graphene-based broadband optical modulator," Nature **474**(7349), 64–67 (2011).
23. W. Li, B. Chen, C. Meng, W. Fang, Y. Xiao, X. Li, Z. Hu, Y. Xu, L. Tong, H. Wang, W. Liu, J. Bao, and Y. R. Shen, "Ultrafast All-Optical Graphene Modulator," Nano Lett. **14**(2), 955–959 (2014).
24. Z. Shi, L. Gan, T.-H. Xiao, H.-L. Guo, and Z.-Y. Li, "All-Optical Modulation of a Graphene-Cladded Silicon Photonic Crystal Cavity," ACS Photonics **2**(11), 1513–1518 (2015).
25. H. Lin, Y. Song, Y. Huang, D. Kita, S. Deckoff-Jones, K. Wang, L. Li, J. Li, H. Zheng, Z. Luo, H. Wang, S. Novak, A. Yadav, C.-C. Huang, R.-J. Shiue, D. Englund, T. Gu, D. Hewak, K. Richardson, J. Kong, and J. Hu, "Chalcogenide Glass-on-Graphene Photonics," Nat. Photonics **11**(12), 798–805 (2017).
26. Z. Sun, T. Hasan, F. Torrisi, D. Popa, G. Privitera, F. Wang, F. Bonaccorso, D. M. Basko, and A. C. Ferrari, "Graphene Mode-Locked Ultrafast Laser," ACS Nano **4**(2), 803–810 (2010).
27. X. Gan, C. Zhao, Y. Wang, D. Mao, L. Fang, L. Han, and J. Zhao, "Graphene-assisted all-fiber phase shifter and switching," Optica **2**(5), 468–471 (2015).
28. T. Cassese, M. A. Giambra, V. Sorianello, G. De Angelis, M. Midrio, M. Pantouvaki, J. Van Campenhout, I. Asselberghs, C. Huyghebaert, A. D'Errico, and M. Romagnoli, "Capacitive actuation and switching of add–drop graphene-silicon micro-ring filters," Photonics Res. **5**(6), 762–766 (2017).
29. P. Avouris, "Graphene: Electronic and Photonic Properties and Devices," Nano Lett. **10**(11), 4285–4294 (2010).
30. T. Gu, N. Petrone, J. F. McMillan, A. van der Zande, M. Yu, G. Q. Lo, D. L. Kwong, J. Hone, and C. W. Wong, "Regenerative oscillation and four-wave mixing in graphene optoelectronics," Nat. Photonics **6**(8), 554–559 (2012).
31. D. Popa, Z. Sun, F. Torrisi, T. Hasan, F. Wang, and A. C. Ferrari, "Sub 200 fs pulse generation from a graphene mode-locked fiber laser," Appl. Phys. Lett. **97**(20), 203106 (2010).
32. X. Li, Y. Zhu, W. Cai, M. Borysiak, B. Han, D. Chen, R. D. Piner, L. Colombo, and R. S. Ruoff, "Large Area, Few-Layer Graphene Films on Arbitrary Substrates by Chemical Vapor Deposition," Nano Lett. **9**(1), 30–35 (2009).
33. L. Wang, X. Zhou, S. Yang, G. Huang, and Y. Mei, "2D-material-integrated whispering-gallery-mode microcavity," Photonics Res. **7**(8), 905–916 (2019).
34. M. Romagnoli, V. Sorianello, M. Midrio, F. H. L. Koppens, C. Huyghebaert, D. Neumaier, P. Galli, W. Templ, A. D'Errico, and A. C. Ferrari, "Graphene-based integrated photonics for next-generation datacom and telecom," Nat. Rev. Mater. **3**(10), 392–414 (2018).
35. Q. Bao and K. P. Loh, "Graphene Photonics, Plasmonics, and Broadband Optoelectronic Devices," ACS Nano **6**(5), 3677–3694 (2012).
36. C. Zheng, X. Jiang, S. Hua, L. Chang, G. Li, H. Fan, and M. Xiao, "Controllable optical analog to electromagnetically induced transparency in coupled high-Q microtoroid cavities," Opt. Express **20**(16), 18319–18325 (2012).
37. C. Yang, X. Jiang, Q. Hua, S. Hua, Y. Chen, J. Ma, and M. Xiao, "Realization of controllable photonic molecule based on three ultrahigh-Q microtoroid cavities," Laser Photonics Rev. **11**(2), 1600178 (2017).
38. A. C. Ferrari, J. C. Meyer, V. Scardaci, C. Casiraghi, M. Lazzeri, F. Mauri, S. Piscanec, D. Jiang, K. S. Novoselov, S. Roth, and A. K. Geim, "Raman Spectrum of Graphene and Graphene Layers," Phys. Rev. Lett. **97**(18), 187401 (2006).
39. M. Cai, O. Painter, and K. J. Vahala, "Observation of Critical Coupling in a Fiber Taper to a Silica-Microsphere Whispering-Gallery Mode System," Phys. Rev. Lett. **85**(1), 74–77 (2000).
40. D. Farnesi, F. Chiavaioli, G. C. Righini, S. Soria, C. Trono, P. Jorge, and G. Nunzi Conti, "Long period grating-based fiber coupler to whispering gallery mode resonators," Opt. Lett. **39**(22), 6525–6528 (2014).
41. D. Farnesi, F. Chiavaioli, F. Baldini, G. C. Righini, S. Soria, C. Trono, and G. N. Conti, "Quasi-distributed and wavelength selective addressing of optical micro-resonators based on long period fiber gratings," Opt. Express **23**(16), 21175–21180 (2015).
42. M. Eichenfield, C. P. Michael, R. Perahia, and O. Painter, "Actuation of micro-optomechanical systems via cavity-enhanced optical dipole forces," Nat. Photonics **1**(7), 416–422 (2007).
43. H. A. Haus, *Waves and Fields in Optoelectronics*, Prentice-Hall, Inc., Englewood Cliffs, NJ, USA 1984.
44. H. Rokhsari and K. J. Vahala, "Ultralow Loss, High-Q, Four Port Resonant Couplers for Quantum Optics and Photonics," Phys. Rev. Lett. **92**(25), 253905 (2004).
45. J. Yao and M. C. Wu, "Bandwidth-tunable add-drop filters based on micro-electro-mechanical-system actuated silicon microtoroidal resonators," Opt. Lett. **34**(17), 2557–2559 (2009).

Optics EXPRESS

46. C. Baker, C. Belacel, A. Andronico, P. Senellart, A. Lemaitre, E. Galopin, S. Ducci, G. Leo, and I. Favero, "Critical optical coupling between a GaAs disk and a nanowaveguide suspended on the chip," Appl. Phys. Lett. **99**(15), 151117 (2011).
47. J. R. Piper and S. Fan, "Total Absorption in a Graphene Monolayer in the Optical Regime by Critical Coupling with a Photonic Crystal Guided Resonance," ACS Photonics **1**(4), 347–353 (2014).
48. V. Sorianello, G. De Angelis, T. Cassese, M. Midrio, M. Romagnoli, M. Mohsin, M. Otto, D. Neumaier, I. Asselberghs, J. Van Campenhout, and C. Huyghebaert, "Complex effective index in graphene-silicon waveguides," Opt. Express **24**(26), 29984–29993 (2016).
49. G. Sinatkas, T. Christopoulos, O. Tsilipakos, and E. E. Kriezis, "Comparative Study of Silicon Photonic Modulators based on Transparent Conducting Oxide and Graphene," Phys. Rev. Appl. **12**(6), 064023 (2019).
50. A. Autere, H. Jussila, Y. Dai, Y. Wang, H. Lipsanen, and Z. Sun, "Nonlinear Optics with 2D Layered Materials," Adv. Mater. **30**(24), 1705963 (2018).
51. L. Reeves, Y. Wang, and T. F. Krauss, "2D Material Microcavity Light Emitters: To Lase or Not to Lase?" Adv. Opt. Mater. **6**(19), 1800272 (2018).
52. H. Fang, J. Liu, Q. Lin, R. Su, Y. Wei, T. F. Krauss, J. Li, Y. Wang, and X. Wang, "Laser-Like Emission from a Sandwiched $MoTe_2$ Heterostructure on a Silicon Single-Mode Resonator," Adv. Opt. Mater. **7**(20), 1900538 (2019).